




Article

Hydroxyl Radical vs. One-Electron Oxidation Reactivities in an Alternating GC Double-Stranded Oligonucleotide: A New Type Electron Hole Stabilization

Annalisa Masi ^{1,†,‡} , Amedeo Capobianco ^{2,†} , Krzysztof Bobrowski ³ , Andrea Peluso ² and Chrysostomos Chatgililoglu ^{1,4,*} 

- ¹ Istituto per la Sintesi Organica e la Fotoreattività, Consiglio Nazionale delle Ricerche, 40129 Bologna, Italy; annalisa.masi@ic.cnr.it
- ² Dipartimento di Chimica e Biologia “A. Zambelli”, Università di Salerno, 84084 Fisciano, Italy; acapobianco@unisa.it (A.C.); apeluso@unisa.it (A.P.)
- ³ Centre of Radiation Research and Technology, Institute of Nuclear Chemistry and Technology, 03-195 Warsaw, Poland; kris@ichtj.pl
- ⁴ Center for Advanced Technologies, Adam Mickiewicz University, 61-614 Poznań, Poland
- * Correspondence: chrys@isof.cnr.it
- † These authors contributed equally to this work.
- ‡ Current address: Istituto di Cristallografia, Consiglio Nazionale delle Ricerche, 00015 Monterotondo, Italy

Abstract: We examined the reaction of hydroxyl radicals (HO•) and sulfate radical anions (SO₄•[−]), which is generated by ionizing radiation in aqueous solutions under anoxic conditions, with an alternating GC double-stranded oligodeoxynucleotide (ds-ODN), i.e., the palindromic 5′-d(GCGCGC)-3′. In particular, the optical spectra of the intermediate species and associated kinetic data in the range of ns to ms were obtained via pulse radiolysis. Computational studies by means of density functional theory (DFT) for structural and time-dependent DFT for spectroscopic features were performed on 5′-d(GCGC)-3′. Comprehensively, our results suggest the addition of HO• to the G:C pair moiety, affording the [8-HO-G:C]• detectable adduct. The previous reported spectra of one-electron oxidation of a variety of ds-ODN were assigned to [G(-H⁺):C]• after deprotonation. Regarding 5′-d(GCGCGC)-3′ ds-ODN, the spectrum at 800 ns has a completely different spectral shape and kinetic behavior. By means of calculations, we assigned the species to [G:C/C:G]•⁺, in which the electron hole is predicted to be delocalized on the two stacked base pairs. This transient species was further hydrated to afford the [8-HO-G:C]• detectable adduct. These remarkable findings suggest that the double-stranded alternating GC sequences allow for a new type of electron hole stabilization via delocalization over the whole sequence or part of it.

Keywords: DNA damage; oligonucleotide; hydroxyl radical; one-electron oxidation; electron hole stabilization; pulse radiolysis; DFT calculations; reaction mechanism



Citation: Masi, A.; Capobianco, A.; Bobrowski, K.; Peluso, A.; Chatgililoglu, C. Hydroxyl Radical vs. One-Electron Oxidation Reactivities in an Alternating GC Double-Stranded Oligonucleotide: A New Type Electron Hole Stabilization. *Biomolecules* **2023**, *13*, 1493. <https://doi.org/10.3390/biom13101493>

Academic Editor: Liang-Jun Yan

Received: 4 September 2023

Revised: 30 September 2023

Accepted: 4 October 2023

Published: 8 October 2023



Copyright: © 2023 by the authors. Licensee MDPI, Basel, Switzerland. This article is an open access article distributed under the terms and conditions of the Creative Commons Attribution (CC BY) license (<https://creativecommons.org/licenses/by/4.0/>).

1. Introduction

Reactive oxygen species (ROS) generated as a result of normal intracellular metabolism include hydroxyl radicals (HO•) that can cause damage to biomolecules [1]. The reaction of HO• with DNA is known to be deleterious in vivo, producing a variety of lesions that have been studied in detail from various points of view, including biophysical, biochemical, biological, and diagnostic approaches [2–4]. The nature of DNA lesions depends on the type of attack, i.e., the hydrogen atom abstraction from the 2′-deoxyribose units or the addition to the base moieties, with the latter being the predominant one (accounting for 85–90% of the attacked sites) [3,5]. The 8-oxo-7,8-dihydro-guanine moiety (8-oxo-G) is a major DNA lesion produced by oxidative stress, and its formation is the result of an initial HO• attack or the one-electron oxidation step [3]. The mechanism of 8-oxo-G formation by the reaction of HO• with calf thymus DNA [6,7] and 21-mer double-stranded oligonucleotides [8] in the

presence of oxygen has been investigated in a few detailed studies. It has been proposed that three pathways contribute to the formation of the 8-oxo-G moiety, with the two major ones being oxygen-dependent [6–8]. The proposed mechanistic scheme reported in Figure 1 consists of directly adding HO• to the C8 position of the guanine moiety, forming 8-HO-G• as the minor path (5–10%) followed by one-electron oxidation. The majority of HO• attacks (90–95%) will be unselective, producing a variety of carbon-centered radicals that, in the presence of O₂, give the corresponding peroxy radicals [5]. It has been suggested that 8-oxo-G is produced by two types of reactions in approximately equal amounts, with both involving DNA–OO• radicals: (1) an intramolecular electron transfer leading to DNA–OO[−] together with the Watson–Crick base pair radical cation [G:C]^{•+} and (2) intramolecular oxidation through the addition of peroxy radicals onto the C8 of a vicinal guanine base [6,7]. Model studies on oligonucleotides have reported the transient generation of pyrimidine peroxy radicals and their addition to the C8 of a vicinal guanine base [9,10]. It is also worth mentioning that Fapy-G lesions are chemically related to 8-oxo-G since they are generated from the same intermediate 8-HO-G•, and their formation depends on the oxygen concentration and the redox environment (Figure 1) [11–13].

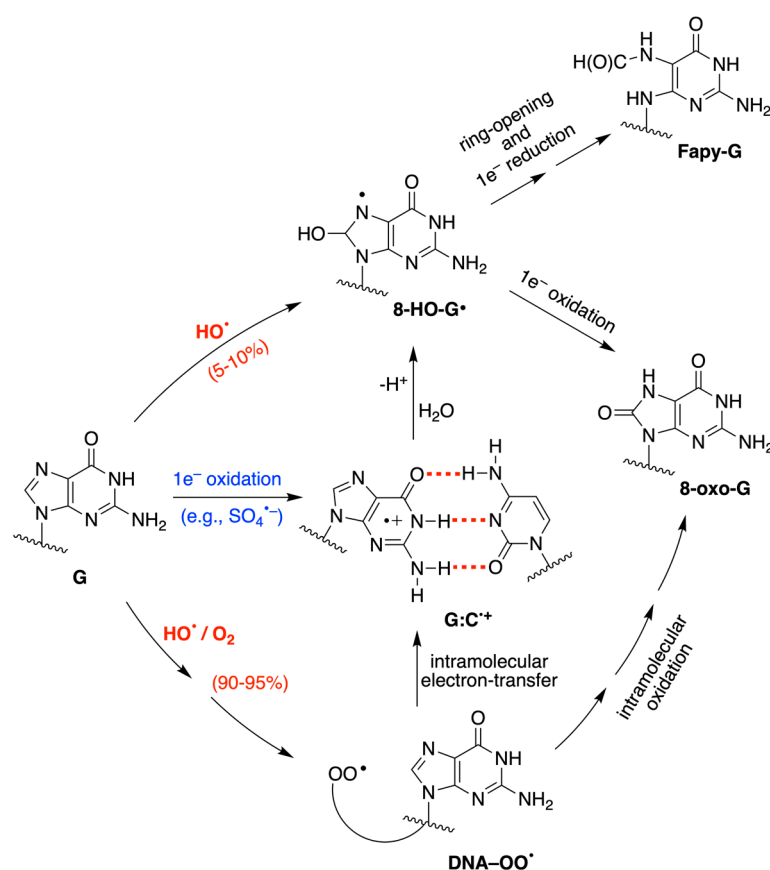


Figure 1. Proposed mechanism for the reactions of HO• and SO₄^{•−} with G moieties in ds-ODNs and DNA; the reactions lead to the formation of 8-oxo-G and Fapy-G as stable lesions [6–8].

The redox properties of nucleobases, nucleosides, nucleotides, and DNA sequences have been investigated via the use of several techniques [14–17]. Liquid jet photoelectron spectroscopy, voltammetry, and quantum chemical calculations find G as the most easily oxidizable nucleobase. The oxidation potential of adenine (A) is estimated to be 0.4 eV higher than guanine, while the pyrimidine moieties of cytosine and thymine (C,T) are oxidized at a potential higher than G (0.6–0.8 eV) [17]. Therefore, the G radical cation (G^{•+}) is considered the putative initial intermediate in the oxidative DNA damage [17–21]. Furthermore, the formation of the Watson–Crick G:C and A:T pairs in chloroform solution

lowers the oxidation potentials of G and A [22,23]; in oligonucleotides containing consecutive G and A homosequences, the formation of delocalized hole domains is possible and has been observed both via voltammetry and time-dependent spectroscopy [24,25]. Particular attention is given to the one-electron oxidation of the G:C pair and the complex mechanism of the deprotonation vs. hydration steps of $[G:C]^{\bullet+}$ pair (Figure 1) [26]. For the hydration reaction of $[G:C]^{\bullet+}$ in DNA, the identification of 8-HO-G \bullet by electron spin resonance (ESR) spectroscopy has been reported [27,28], and information on the reaction mechanism has also been reported [29]. To our knowledge, the water trapping rate of $[G:C]^{\bullet+}$ has not been measured yet, but a pseudo-first-order rate constant was estimated to be $6 \times 10^4 \text{ s}^{-1}$ via an indirect method in [30]. Moreover, there have been numerous studies on the formation and behavior of G \bullet in ds-ODNs using spectroscopic and product studies [31].

It is worth mentioning that the role of HO \bullet in redox processes with DNA is not well understood. Evidence has suggested that HO \bullet and one-electron oxidants may partly induce common degradation pathways [32]. Very often, the description of this chemistry is simplified by reporting the known chemistry of corresponding nucleosides. However, the reaction of HO \bullet with the four bases of DNA in a macromolecular environment is quite different from the reaction of HO \bullet with simple nucleosides. Indeed, an ambident reactivity has been observed for the reaction of HO \bullet with the G moiety of 2'-deoxyguanosine (2'-dGuo) in aqueous medium [33,34]. The main pathway (~65%) involves H-atom abstraction from the exocyclic NH₂ group followed by water-assisted tautomerization [35], whereas the minor pathway is the direct addition at the C8 position, resulting in the formation of the adduct radical (17%). H-atom abstraction from the sugar moiety (~18%) completes the picture, half of which occurs at the H5' positions, followed by radical cyclization with the formation of 5',8-cyclo-2'-deoxyguanosine [3,36]. On the other hand, the reaction of HO \bullet with 2'-deoxycytidine (2'-dCyd) occurs via addition at C5 and C6 positions in a ca. ratio of 90:10. Experimental evidence regarding H-atom abstraction from amino groups and/or sugar moieties is not available [37], although evidence that the aminyl radical tautomerizes to the most stable forms has been presented [38,39].

The present study provides spectral and kinetic data (obtained via pulse radiolysis) for the various intermediates from the reactions of HO \bullet and SO₄ \bullet^- using an alternating GC double-stranded 6-mer oligonucleotide, i.e., the ds-ODN of the palindromic 5'-d(GCGCGC)-3', in deoxygenated aqueous solutions in a condition that excludes the main reactions of HO \bullet /O₂ of Figure 1. This model sequence is also connected with the DNA reactivity, especially with respect to the GC-rich isochores, which are characterized by a high gene density [40,41]. We also theoretically address the reactivity of the G:C complex with HO \bullet by considering all the possible HO \bullet additions and H-atom abstraction from the -NH₂ group to both G and C moieties, as well as outer-sphere electron transfer from the whole G:C complex to SO₄ \bullet^- . Moreover, the double-stranded 5'-d(GCGCGC)-3' B-DNA sequence was used as a model compound for the theoretical analysis of one-electron-oxidized ds-ODN. Our results are discussed in comparison with other time-resolved spectroscopic studies reported for the reaction of SO₄ \bullet^- with similar ds-ODNs [42–46]. We show that interstrand hydrogen bonds can significantly affect the reactivity of HO \bullet with G and C in ds-ODN. Additionally, alternating GC ds-ODN has a remarkable effect on the delocalization of the radical cation and the reaction outcome.

2. Materials and Methods

2.1. Preparation of Double-Stranded Oligonucleotide (ds-ODN)

The oligonucleotide 5'-d(GCGCGC)-3' was prepared and purified following protocols described previously [47]. To obtain the ds-ODN, the palindromic strand 5'-d(GCGCGC)-3' was annealed in buffer solution containing 50 mM sodium phosphate (NaH₂PO₄). The substrate was constructed by using a previously reported procedure, showing a melting temperature (T_m) of 45.9 °C [47]. Analyzing the melting curve at 20 °C, the temperature at which the pulse radiolysis experiments are performed, a percentage of 87% of ds-ODN was estimated (see Supplementary Materials for details).

2.2. Pulse Radiolysis

The experiments with time-resolved UV-vis optical absorption detection were carried out at the Institute of Nuclear Chemistry and Technology in Warsaw, Poland. The linear electron accelerator (LAE 10), which delivered 10 ns pulses with an electron energy of about 10 MeV, was applied as a source of irradiation. A detailed description of the experimental setup has been given elsewhere, along with basic details of the equipment and its data collection system [48]. A 150 W xenon arc lamp E7536 (Hamamatsu, Shizuoka, Japan) was used as a monitoring light source. The respective wavelengths were selected by using a MSH 301 (Lot Oriel Gruppe, Darmstadt, Germany) motorized monochromator/spectrograph with two optical output ports. The time-dependent intensity of the analyzing light was measured via means of photomultiplier (PMT) R955 (Hamamatsu, Shizuoka, Japan). A detector signal was digitized using a WaveSurfer 104MXs-B (1 GHz, 10 GS/s, LeCroy) oscilloscope. A water filter was used to eliminate near-IR wavelengths. The optical path of the microcells was 1 cm, with a total volume of irradiated solution of about 300 μL . All experiments were carried out at ambient temperature (~ 20 °C). The spectral range that can be covered with the existing pulse radiolysis set-up is between 300 and 700 nm. The dosimetry was based on N_2O -saturated solutions containing 10 mM KSCN, which, following radiolysis, produces $(\text{SCN})_2^{\bullet-}$ radical anions that have a molar absorption coefficient of $7580 \text{ M}^{-1} \text{ cm}^{-1}$ at $\lambda = 472 \text{ nm}$ and are produced with a radiation chemical yield of $G = 0.635 \mu\text{mol J}^{-1}$ [49]. Absorbed doses per pulse were on the order of about 20 Gy (1 Gy = 1 J kg^{-1}).

2.3. Computational Details

Equilibrium geometries of the species were evaluated at the density functional level of theory (DFT) using the B3LYP functional with the 6-311++G(d,p) basis set [50]. The Hessian matrix was systematically computed to ascertain the location of the stationary points corresponding to the minimum geometry structures. Solvent (water) effects were included in all computations. The polarizable continuum model (PCM) with standard parameters was used throughout [51]. The unrestricted formalism was adopted for species with unpaired electrons. For reaction products, the wavelengths and oscillator strengths of excited states were predicted via time-dependent (TD) DFT computations by using the same functional and basis set employed for the geometry optimizations.

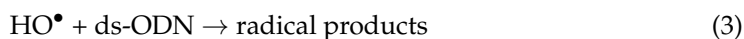
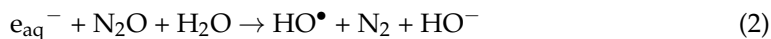
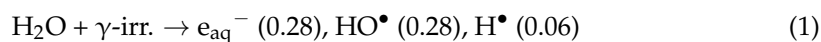
The starting geometry of the ds-5'-GCGC-3' DNA sequence was prepared in B-form using 3DNA (version 2.2). Based on calf thymus conformations, the default model of B-DNA was adopted [52]. The negative charge of phosphate units was neutralized by sodium ions [24]. Then, the geometry of $[\text{ds-5'-GCGC-3'}]^{\bullet+}$, i.e., ds-5'-GCGC-3' oxidized via the removal of a single electron, was optimized at the PCM/DFT level of theory in conjunction with the D3BJ (B3LYP-D3BJ) empirical correction for dispersion energy [53]. The TZVP basis set was used because it has been shown to predict very reliable geometries for short DNA sequences, reaching almost the same quality as more extensive basis sets [54]. The $[\text{ds-5'-GCGC-3'}]^{\bullet+}$ oxidized oligonucleotide was also investigated at the PCM-CAM-B3LYP-D3BJ/TZVP level of computation [55]. After geometry optimizations were carried out at the PCM/B3LYP-D3BJ/TZVP level, TD-B3LYP/TZVP computations were carried out for $^{\text{me}}\text{G}^{\bullet+}$, the $[\text{meG:C}^{\text{me}}]^{\bullet+}$ Watson and Crick complex, and the $[\text{meG:C}^{\text{me}}/\text{meC}^{\text{me}}\text{G}]^{\bullet+}$ stack. The latter system was also investigated at the PCM/TD-CAM-B3LYP/TZVP level. All DFT and TDDFT computations were carried out by using the Gaussian package [56].

3. Results

3.1. Pulse Radiolysis Study

Radiolysis of neutral water leads to the reactive species e_{aq}^- , HO^\bullet , and H^\bullet , as shown in Reaction 1. The values in parentheses represent the radiation chemical yields (G) in units

of $\mu\text{mol J}^{-1}$. In N_2O -saturated solution (~ 0.02 M of N_2O), e_{aq}^- are converted into HO^\bullet radicals via Reaction 2 ($k_2 = 9.1 \times 10^9 \text{ M}^{-1} \text{ s}^{-1}$), with $G(\text{HO}^\bullet) = 0.56 \mu\text{mol J}^{-1}$ [57,58].



The reaction of HO^\bullet with the palindromic 5'-d(GCGCGC)-3' doubled-stranded oligonucleotide (ds-ODN) was investigated in phosphate-buffered (50 mM) N_2O -saturated solutions of 0.134 mM ds-ODN at natural pH (pH 7 was recorded). Transient absorption spectra in the range of 300–700 nm recorded at 4.8, 60, and 1000 μs after the electron pulse are presented in Figure 2. The transient spectrum obtained at 4.8 μs shows a dominant absorption band ($\lambda = 310$ nm) that constantly decreases up to 700 nm with a weak shoulder in the 400–450 nm range. The spectrum recorded at 60 μs is slightly less intensive and did not show any relevant change in the 300–700 nm range. With the further elapse of time, the spectrum observed at 1000 μs exhibited a strong band with no distinct λ_{max} at wavelengths in the range of 300–700 nm. A rate constant of $1.4 \times 10^{10} \text{ M}^{-1} \text{ s}^{-1}$ was determined for Reaction 3 by measuring the pseudo-first-order rate constant of the increase in the absorbance at $\lambda_{\text{max}} = 310$ nm for the specified concentration of ds-ODN (0.134 mM) and assigned to the main transient formed (the top inset of Figure 2). In turn, its disappearance followed first-order kinetics, with $k = 1.6 \times 10^3 \text{ s}^{-1}$ (see the bottom inset of Figure 2).

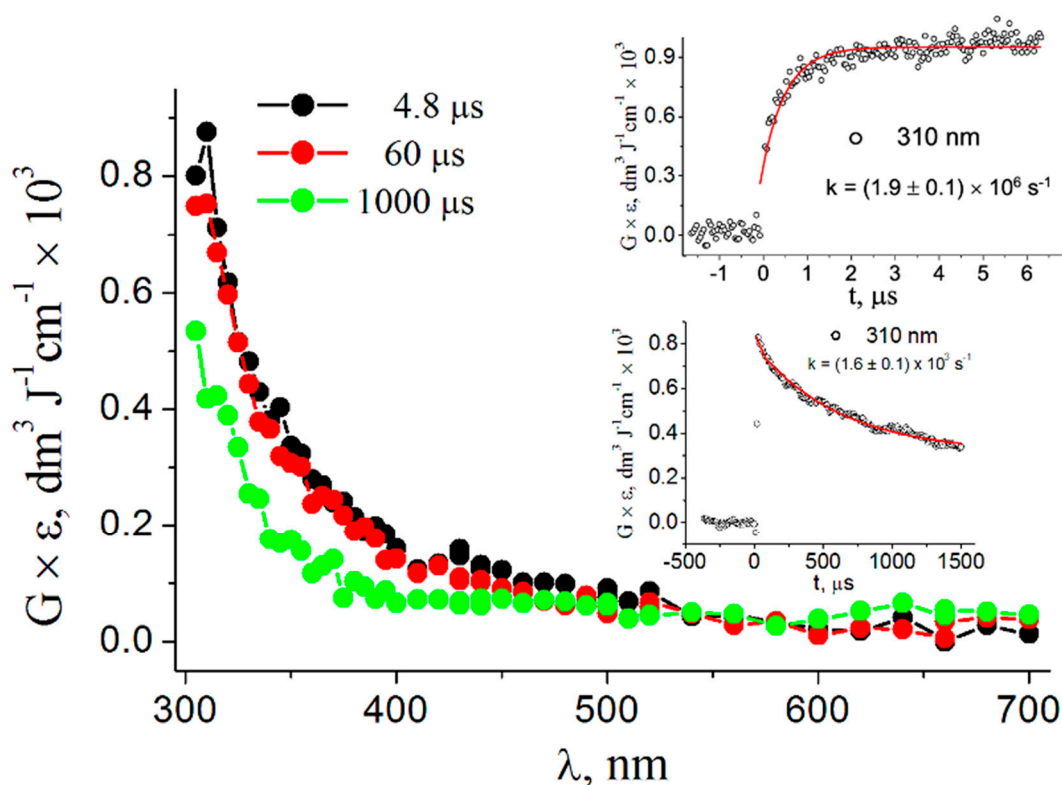


Figure 2. Absorption spectra obtained from the pulse radiolysis of a N_2O -saturated phosphate-buffered (50 mM) solution containing 0.134 mM ds-ODN at pH 7 (taken at 4.8, 60, and 1000 μs after the electron pulse). Inset: Time dependence of absorption at 310 nm (build-up and decay) recorded in the same experimental conditions of the spectra; the red lines represent the first-order kinetic fit to the data.

The sulfate radical anion $\text{SO}_4^{\bullet-}$ was generated by irradiating an Ar-purged solution containing 20 mM of ammonium persulfate in the presence of 0.1 M of tert-butanol; under these

conditions, e_{aq}^- and H^\bullet are converted into $SO_4^{\bullet-}$ via Reaction 4 ($k_4 = 1.2 \times 10^{10} \text{ M}^{-1} \text{ s}^{-1}$) and Reaction 5 ($k_5 = 2.5 \times 10^7 \text{ M}^{-1} \text{ s}^{-1}$), respectively, whereas HO^\bullet radicals are scavenged by the alcohol (Reaction 6) [57].

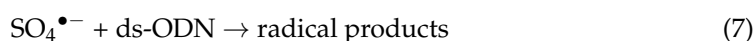
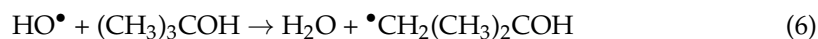
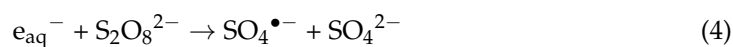


Figure 3 shows the optical absorption spectra of $SO_4^{\bullet-}$ (black circles) and the new transient spectrum obtained from the reaction with ds-ODN (red circles) (taken at 32 ns and 800 ns after the electron pulse, respectively). The rate constant of $8.2 \times 10^{10} \text{ M}^{-1} \text{ s}^{-1}$ was determined for the reactions of $SO_4^{\bullet-}$ with ds-ODN at pH 7 (Reaction 7) by measuring the growth of absorbance of a new transient species at $\lambda_{max} = 330 \text{ nm}$ (the top inset of Figure 3). Furthermore, the disappearance of this species gives rise to another transient, the spectrum of which (taken at 60 μs after the pulse) is also shown in Figure 3 (green circles). A first-order rate constant of $1.5 \times 10^5 \text{ s}^{-1}$ was measured for the transformation of the red spectrum to the green one by following the rate of the decrease in absorbance at $\lambda = 330 \text{ nm}$ (see the bottom inset of Figure 3).

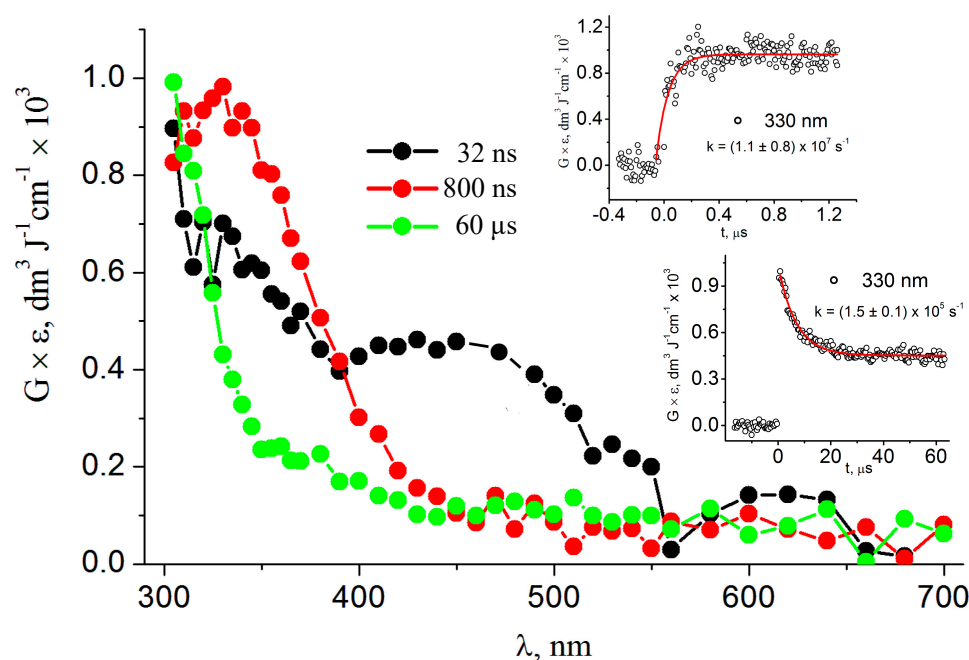


Figure 3. Absorption spectra obtained from the pulse radiolysis of an Ar-purged phosphate-buffered (50 mM) solution containing 0.134 mM ds-ODN, 20.0 mM ammonium persulfate, and 0.1 M tert-butanol at pH 7 (taken at 32 ns, 800 ns, and 60 μs after the pulse). Inset: Time dependence of absorbance at 330 nm (build-up and decay) (recorded in the same experimental conditions of the spectra); the red lines represent the first-order kinetic fit to the data.

Figure 4 presents the optical absorption spectra of the two transients obtained by reactions of HO^\bullet (red circles) and $SO_4^{\bullet-}$ (black circles) with ds-ODN taken at 1000 μs after the pulse, taking into consideration the radiation chemical yields (G) of the two reactive species. It is gratifying to see that the two spectra are nearly identical in terms of feature and intensity. Moreover, the disappearance of both transients observed at $\lambda = 310 \text{ nm}$ followed first-order kinetics, with the two having similar first-order rate constants of

$1.6 \times 10^3 \text{ s}^{-1}$ and $1.1 \times 10^3 \text{ s}^{-1}$ for the reactions of HO^\bullet (red circles) and $\text{SO}_4^{\bullet-}$ (black circles), respectively (see insets in Figure 4).

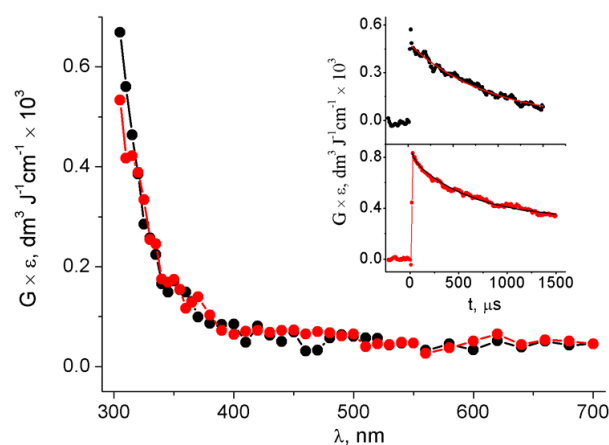


Figure 4. Comparison of the absorption spectra obtained via pulse radiolysis from the reaction of 0.134 mM ds-ODN with HO^\bullet (red circles) and $\text{SO}_4^{\bullet-}$ (black circles) in phosphate-buffered (50 mM) solution at pH 7 (taken at 1000 μs after the pulse). Insets: Time dependence of absorbance at $\lambda = 310 \text{ nm}$, which was recorded in the same experimental conditions as the transient spectra obtained from the reaction involving $\text{SO}_4^{\bullet-}$ (top inset) and HO^\bullet (bottom inset) radicals.

3.2. Theoretical Calculations

The reactivity of the Watson–Crick G:C complex with HO^\bullet has been previously considered [59–61]. HO^\bullet addition to the C4, C5, and C8 carbon sites of G the moiety and to the C5 and C6 carbons of the C moiety (see Figure 5 for atom numbering, where sugar-phosphate moieties have been replaced by methyl groups (viz., $^{\text{me}}\text{G}:\text{C}^{\text{me}}$)) leads to stable adducts with respect to possible proton transfer processes within the G:C pair. The addition of HO^\bullet to the C8 of $^{\text{me}}\text{G}$ has been predicted to be the most favored process. Previous computations have also predicted that the addition of HO^\bullet to the C5 and C6 sites of $^{\text{me}}\text{C}$ are more favored than those to the C4 and C5 of $^{\text{me}}\text{G}$. This has been traced back to the significant distortion from planarity of the whole G ring upon the addition of HO^\bullet to the C4 and C5 sites of G [59]. Our own computations confirmed all of these results, cf. Table 1 for the predicted energy changes (ΔE , kcal/mol); furthermore, no barriers were predicted for any of the HO^\bullet addition reactions. A desolvation barrier could be expected since HO^\bullet is significantly solvated in water [62,63], but it could hardly discriminate among the different sites of the G:C complex; thus, it was not expected to affect the selectivity of HO^\bullet addition toward the different sites of the G:C complex.

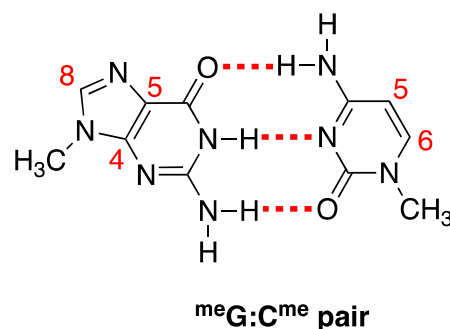


Figure 5. Adopted atom numbering of the $^{\text{me}}\text{G}:\text{C}^{\text{me}}$ pair.

Table 1. Predicted energy changes (ΔE , kcal/mol) for the addition of HO• to ^{me}G:C^{me} pairs in water and for H-atom abstraction from the NH₂ moieties of G or C by HO•; the absorption wavelengths (λ , nm) and oscillator strengths (f) of all the HO• adducts in water are also shown.

| $\Delta E = -31.7$ | | $\Delta E = -9.9$ | | $\Delta E = -15.0$ | | $\Delta E = -21.7$ | | $\Delta E = -17.3$ | | $\Delta E = -18.6$ | | $\Delta E = -9.4$ | |
|--------------------|-------|-------------------|-------|--------------------|-------|--------------------|-------|--------------------|-------|--------------------|-------|-------------------|-------|
| λ , nm | f | λ , nm | f | λ , nm | f | λ , nm | f | λ , nm | f | λ , nm | f | λ , nm | f |
| 430 | 0.019 | 535 | 0.008 | 481 | 0.007 | 595 | 0.006 | 420 | 0.065 | 808 | 0.003 | 1788 | 0.003 |
| 397 | 0.021 | 483 | 0.074 | 437 | 0.009 | 570 | 0.001 | 346 | 0.024 | 632 | 0.015 | 874 | 0.033 |
| 386 | 0.002 | 402 | 0.033 | 399 | 0.005 | 567 | 0.079 | 313 | 0.002 | 488 | 0.021 | 338 | 0.028 |
| 376 | 0.040 | 381 | 0.006 | 377 | 0.014 | 482 | 0.007 | 312 | 0.028 | 413 | 0.002 | 270 | 0.011 |
| 353 | 0.002 | 363 | 0.036 | 362 | 0.054 | 447 | 0.011 | | | 373 | 0.001 | 265 | 0.108 |
| 339 | 0.010 | 360 | 0.053 | 356 | 0.017 | 350 | 0.056 | | | 368 | 0.001 | | |
| 325 | 0.041 | 340 | 0.005 | 350 | 0.059 | 309 | 0.085 | | | 324 | | | |
| 309 | 0.073 | 328 | 0.003 | 347 | 0.038 | | | | | | | | |
| 308 | 0.019 | 321 | 0.011 | 337 | 0.034 | | | | | | | | |

We also considered H-atom abstraction by HO• from the -NH₂ group of both G and C. As expected [33,34], H-atom abstraction from the exocyclic amino group of ^{me}G was predicted to be significantly more favored than that from ^{me}C (Table 1, columns 4 and 7). No barriers have been found for both processes. H-atom abstraction from G takes place even when HO• is completely surrounded by the water molecules of its first solvation shell via the network of H-bonds connecting the solvated HO• to the amino group of G. Even though H-atom abstraction from the G moiety is less exergonic than HO• addition to C8, the former process is expected to be entropically favored in water solution. Evaluating reliable entropic changes in solution at this level of computation is not possible, and calculating ΔG is a highly demanding computational task [64]. Here, it is important to note that the large internal energy gain (ca. 10 kcal/mol), which favors HO• addition to C8 with respect to H-atom abstraction, can be much smaller when Gibbs free energies are considered.

The spectroscopic features of all the HO• adducts were predicted by using time-dependent density functional theory (TDDFT); the absorption wavelengths (λ) and oscillator strengths (f) of the most intense transitions are reported in Table 1. All the HO• adducts exhibit absorptions in the visible region. In particular, the TDDFT computations predicted for the C8 adduct show two intense absorptions at the highest energy region of the visible spectrum—430 and 397 nm with f of 0.019 and 0.021, respectively—and three much more intense absorptions at 376, 325, and 309 nm, with f of 0.040, 0.041 and 0.073, respectively (Table 1, column 1). The situation is somehow different for the HO• adduct formed at the C6 carbon of the cytosine moiety (the second most stable adduct). In that case, TDDFT predicted a very weak absorption at 808 nm and a more intense one at 632 nm, with $f = 0.015$ (Table 1, column 6); those absorptions occurring at longer wavelengths have no counterpart for any other HO• adduct. The most intense electronic transitions predicted by the TDDFT computations are those for the neutral aminyl radicals of both the G and C moieties (Table 1, columns 4 and 7). For G(-H):C, two relevant transitions are predicted in the visible region: a comparatively stronger absorption at 567 nm ($f = 0.079$) and a weaker one at 447 nm ($f = 0.011$). The most intense transition falls in the UV region, being predicted at 309 nm, with $f = 0.085$. The predicted spectrum agrees quite well with that obtained via the pulse radiolysis of the G water solution at neutral pH. For the GC(-H) complex, the predicted absorption spectrum is very different, exhibiting a very weak transition in the NIR region (at 1788 nm), a second, more intense transition at 874 nm ($f = 0.033$), and an intense transition at 338 nm ($f = 0.028$).

We have also considered the addition of $\text{SO}_4^{\bullet-}$ to the C8 site of $^{\text{me}}\text{G}$ and to the C5 and C6 of $^{\text{me}}\text{C}$, as well as the spectroscopic features of the adducts. The results, which are summarized in Table S2 of the Supplementary Materials, indicate much less exergonic reactions.

Although HO^{\bullet} radicals can oxidize DNA nucleobases via inner-sphere electron transfer (ET), which occurs via radical addition to a carbon atom of the G:C complex followed by HO^- elimination, the $\text{SO}_4^{\bullet-}$ is known to act via outer-sphere ET. Initially, we considered a model in which the first hydration shell of $\text{SO}_4^{\bullet-}$ and its ET products were explicitly included in the computation. The optimized structure for $\text{SO}_4^{\bullet-}$ is shown in Figure S3 of the Supplementary Materials. We assumed a tetrahedral arrangement of water molecules around each oxygen atom, considering twelve water molecules for $\text{SO}_4^{\bullet-}$, without attempting to verify whether larger models could be more appropriate. Bulk solvent effects were considered by the polarizable continuum model (PCM) model. As expected, with the inclusion of specific interactions with solvent molecules, ET is predicted to be significantly exergonic for $\text{SO}_4^{\bullet-}$ ($\Delta E = -26.7$ kcal/mol). The above energy change for the outer-sphere ET reaction is in line with those inferred from the standard redox potentials of $\text{SO}_4^-/\text{SO}_4^{2-}$ and guanosine 5'-monophosphate (GMP) GMP^+/GMP (pH 7) semi-couples, which, according to cyclic voltammetry, are 2.60 and 1.31 V (vs. SHE), respectively [65,66]. In summary, outer-sphere ET from the G:C complex to $\text{SO}_4^{\bullet-}$ is predicted to be the most favored process, being largely more exergonic than the direct addition to both the G and C moieties.

Regarding the spectroscopic properties of the $[\text{G:C}]^{\bullet+}$, they have been reported previously [67,68]: a long wavelength absorption is predicted in the NIR region of the spectrum at $11,218\text{ cm}^{-1}$ ($f = 0.006$) and observed at $10,200\text{ cm}^{-1}$ [67], together with two more intense absorptions at 528 nm ($f = 0.019$) and at 370 nm ($f = 0.081$). However, in the case of the present study, the UV absorption spectrum could significantly differ from that of a single G:C pair because the radical cation of ds-ODN of the palindromic 5'-d(GCGCGC)-3' sequence could, in principle, be delocalized over the whole double strand or over a part (the central one) of it. Delocalized hole domains have been experimentally found both in single and double strands containing sequences of consecutive adenines [25,69] and theoretically predicted by DFT computations [24,70]. In the case of G-rich ODN, the situation is less clear inasmuch as differential pulse voltammetries of guanine-rich oligonucleotides containing up to six consecutive guanines showed a progressive decrease in the first voltammetric peak potential as the number of adjacent guanines increased, indicating the establishment of delocalized hole domains [25], whereas ab-initio and DFT computations including solvent effects predict that the hole is localized over a single G, the one located at the 5' side [71,72].

The double-stranded 5'-d(GCGC)-3' palindromic B-DNA sequence was used as a model compound for the theoretical analysis of one-electron oxidized ds-ODN. The predicted (B3LYP) spin density of this oxidized model is depicted in Figure 6. Both B3LYP and CAM-B3LYP (see Supplementary Materials, Figure S2) functionals find the positive charge almost equally distributed over the central guanines. Indeed, Mulliken spin densities of central guanines are predicted to be 0.50, 0.48 by B3LYP and 0.48, 0.52 by CAM-B3LYP. Therefore, computations suggest that states with the hole fully localized on a single guanine are sufficiently coupled with each other to overcome solvent effects that favor charge localization [72,73]. Such a result is remarkable because, in single-stranded DNA oligomers ss-5'-XGGY-3' (X,Y = C,T,A, and 6-azauracil), the electron hole is never predicted to be delocalized on the two stacked guanines [72].

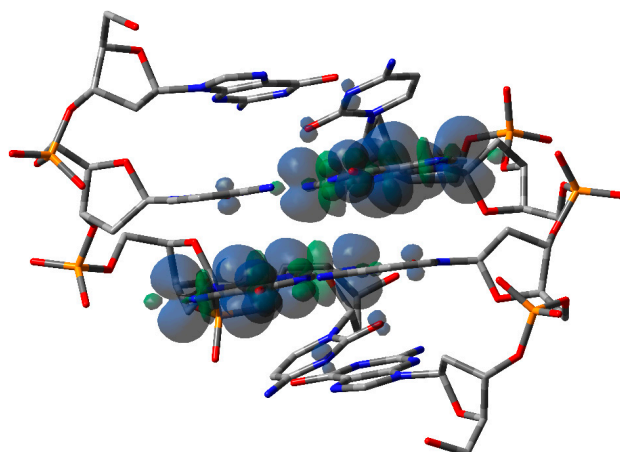


Figure 6. Optimized geometry and spin density plot (PCM/B3LYP-D3BJ/TZVP) of [ds-5'-GCGC-3']^{•+}. Hydrogen atoms and sodium counterions have been omitted for clarity.

In order to make TDDFT computations feasible, sugar phosphate moieties were replaced by methyl groups (viz., ^{me}G:C^{me}). A partial geometry optimization was carried out at the PCM/B3LYP-D3/TZVP level by starting from the optimized geometry of ds-GCGC and only relaxing the atoms of the methyl groups. The lowest energy electronic transition of the alternating GC pairs [^{me}G:C^{me}/^{me}C:G^{me}]^{•+} was predicted by B3LYP computations to occur at 1839 nm, i.e., $\Delta E = 0.67$ eV. This HOMO–LUMO intense absorption involves π MOs with electron densities equally delocalized over the guanines. By using a simple two-state model, such an absorption energy would yield an electronic coupling term between the fully localized diabatic states roughly amounting to 0.33 eV, suggesting that the geometrical arrangement of guanines is very effective in stabilizing the positive charge in oxidized B-DNA sequences composed by alternating GC pairs. CAM-B3LYP (see Figure S4 and Table S5) also finds an intense lowest energy transition involving MOs with charge equally distributed on guanines. However, a substantially lower absorption energy $\Delta E = 0.20$ eV is predicted by the latter functional. A spectroscopic analysis of oxidized ds-ODN in the near- and medium-IR spectral region would be highly advisable to ascertain the effectiveness of interacting guanines in stabilizing the hole in the alternating GC sequences.

The predicted spectrum of [^{me}G:C^{me}/^{me}C:G^{me}]^{•+} is reported in Figure 7 (red line), together with the signal of Figure 3, which was recorded at 800 ns after the pulse. Apart from the intense absorption in the region of the longer wavelength, attributed to the HOMO–LUMO transition, with both levels delocalized over the central guanines, the predicted spectrum exhibits intense absorptions only at significantly shorter wavelengths, i.e., below 270 nm. All the computed transitions are reported in the Supplementary Materials Tables S3–S5, together with the results of previous computations concerning the single radical cation ^{me}G^{•+} and the Watson–Crick [^{me}G:C^{me}]^{•+} complex, whose observed spectra have been reported in the literature, thus being extremely useful for assessing the accuracy of the predicted transition energies. The comparison between the observed and calculated spectra of those latter species shows that the TDDFT computations largely overestimate excitation energies at shorter wavelengths, as also reported by other authors [46,68]. Notwithstanding, the TDDFT computations correctly predict a blue shift of the most intense signal and an increase in the intensity of the most intense absorption with respect to signals at longer wavelengths. Although most of the predicted transitions for [^{me}G:C^{me}]^{•+} involve the π system of guanine, the higher intensity observed for [Guo:dCyd]^{•+} with respect to Guo^{•+} in the region around 300 nm is ascribed by the TDDFT computations to $\pi \rightarrow \pi^*$ transitions that also involve cytosine. This effect is dramatically enhanced in oxidized alternating GC sequences. Indeed, the predicted spectrum of [^{me}G:C^{me}/^{me}G:C^{me}]^{•+} is characterized by a very high ratio between the intensity at 260 nm and the one at 375 nm with respect to the spectra of [^{me}G:C^{me}]^{•+} or ^{me}G^{•+}. That high intensity is ascribed by the TDDFT computa-

tions to the strong coupling between oxidized guanines, which gives rise to several intense absorptions between 260 and 275 nm, involving the G/G π system. Furthermore, the intense $\pi \rightarrow \pi^*$ absorptions of the C/C subsystem, together with charge transfer transitions, moving the hole from the G/G to the C/C units, and transitions that localize the hole on a single G moiety, are predicted in the highest energy region, making the absorption signal even more intense.

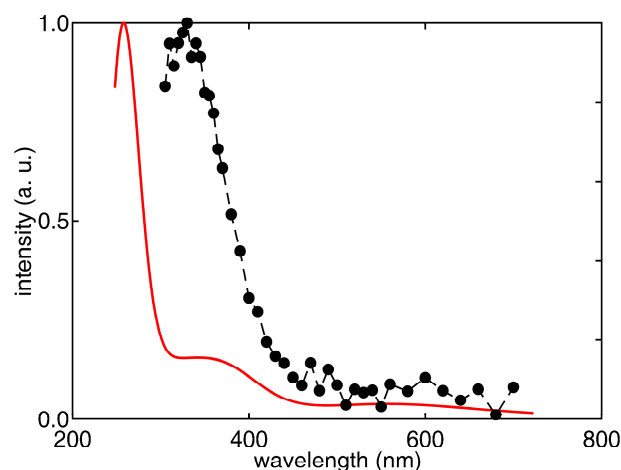


Figure 7. Predicted (PCM-TD-B3LYP/TZVP) UV/vis spectrum of $[\text{meG:C}^{\text{me}}/\text{meC:G}^{\text{me}}]^{\bullet+}$ (red line); vertical transitions have been enlarged by Gaussian functions with full width at half-maximum, amounting to 6000 cm^{-1} , and the heights have been scaled according to the predicted oscillator strengths of Table S2 in the Supplementary Materials. The absorption spectra obtained from the pulse radiolysis of Ar-purged ds-ODN with ammonium persulfate (taken at 800 ns after the exciting pulse) are also shown for comparison (black curve).

4. Discussion

The rate constants for the reactions of HO^\bullet with 2'-deoxyguanosine (2'-dGuo) and 2'-deoxycytidine (2'-dCyd) were found to be similar (Table 2). We measured the rate constant of HO^\bullet with the alternated GC ds-ODN to be $1.4 \times 10^{10} \text{ M}^{-1} \text{ s}^{-1}$. Assuming that the six G:C pairs in ds-ODN of the palindromic 5'-d(GCGCGC)-3' have similar reactivities, we calculated a value of $2.3 \times 10^9 \text{ M}^{-1} \text{ s}^{-1}$ for the reaction of HO^\bullet with the G:C pair, which is approximately five-fold smaller than the sum of the two single nucleoside values participating in the pair. On the other hand, taking into account the concentration of the phosphate buffer (50 mM) used in our study, this rate constant is nearly three-fold larger than the value measured for the ct-DNA [74].

Table 2. Rate constants for the reactions of HO^\bullet and $\text{SO}_4^{\bullet-}$ with 2'-dGuo, 2'-dCyd, and the G:C pair in ds-ODN.

| Substrate | $k(\text{HO}^\bullet), \text{M}^{-1} \text{ s}^{-1}$ | $k(\text{SO}_4^{\bullet-}), \text{M}^{-1} \text{ s}^{-1}$ |
|---------------------------------|--|---|
| 2'-dGuo ¹ | 5.7×10^9 | 4.1×10^9 |
| 2'-dCyd ¹ | 5.6×10^9 | 1.6×10^9 |
| G:C pair in ds-ODN ² | 2.3×10^9 | 13.6×10^9 |

¹ Taken from [5]. ² Present work.

The rate constant for the reactions of $\text{SO}_4^{\bullet-}$ with 2'-dGuo is reported to be 2.5-fold faster than that with 2'-dCyd (Table 2). We measured the rate constant of $\text{SO}_4^{\bullet-}$ with the alternated GC ds-ODN to be $8.2 \times 10^{10} \text{ M}^{-1} \text{ s}^{-1}$. Assuming that the six G:C pairs in ds-ODN have similar reactivities, we calculated a value of $13.6 \times 10^9 \text{ M}^{-1} \text{ s}^{-1}$ for the reaction of $\text{SO}_4^{\bullet-}$ with the G:C pair, which is 3.3- and 8.5-fold larger than the value for the single nucleoside 2'-dGuo and 2'-dCyd and ~2.5-fold larger than the sum of the two single

nucleoside values participating in the pair. Interestingly, this value is very close to the rate constants of the reactions of $\text{SO}_4^{\bullet-}$ with the 30mer ODN containing G moieties in ss-ODNs and ds-ODN [43].

Based on the present study's time-resolved spectroscopy results and theoretical calculations, we assigned the observed spectrum at 4.8 μs for the reaction of HO^\bullet with ds-ODN (Figure 2), i.e., the absorption band with $\lambda = 310$ nm that constantly decreases up to 700 nm, to HO^\bullet radical adduct [8-HOG:C] $^\bullet$ (cf. Figure 8). A clean UV-vis spectrum of the HO^\bullet -adduct to the C8 position of guanine derivatives, i.e., 8-HO-G $^\bullet$, is unknown. An indirect experiment (resulting from the spectra subtraction) and theoretical calculation indicated an intense band near 300 nm, with a broad shoulder up to 500 nm, containing a less intense band between 400 and 450 nm [33]. This description fits well with the recorded spectrum at 4.8 μs in Figure 2. However, we cannot exclude the notion that the weakly pronounced shoulder in the 400–450 nm range may be also due to HO^\bullet adducts either at G5 and/or C5, based on the predicted absorption wavelengths and oscillator strengths reported in Table 1. Interestingly, the broad absorption band with $\lambda_{\text{max}} \approx 600$ nm was not observed at short times, suggesting that HO^\bullet radicals do not react with ds-ODN via H-atom abstraction from the exocyclic NH_2 group in the guanine (G) moiety but rather via addition to the C8 position [30]. However, the observed spectrum matches quite nicely with the transient spectra resulting from the reaction of HO^\bullet radicals with ct-DNA [74] and 12-mer ds-ODN [75]. The absence of H-atom abstraction from the exocyclic NH_2 group in the guanine (G) moiety might result from the specific structure of ds-ODN, which does not allow HO^\bullet radicals to reach the NH_2 moiety [76], as also suggested for 12-mer ds-ODN [75]. A similar though slightly less intense spectrum was recorded at 60 μs , indicating no trace of H-atom abstraction from the C5' position with subsequent radical cyclization to the C8 position in our pulse radiolysis study, as has been previously noted [75]; however, this certainly exists in the background, as demonstrated by numerous product studies [8]. Indeed, this sequence of reactions in naked DNA or ds-ODN is expected to account for the 1–2% of the whole HO^\bullet reactivity.

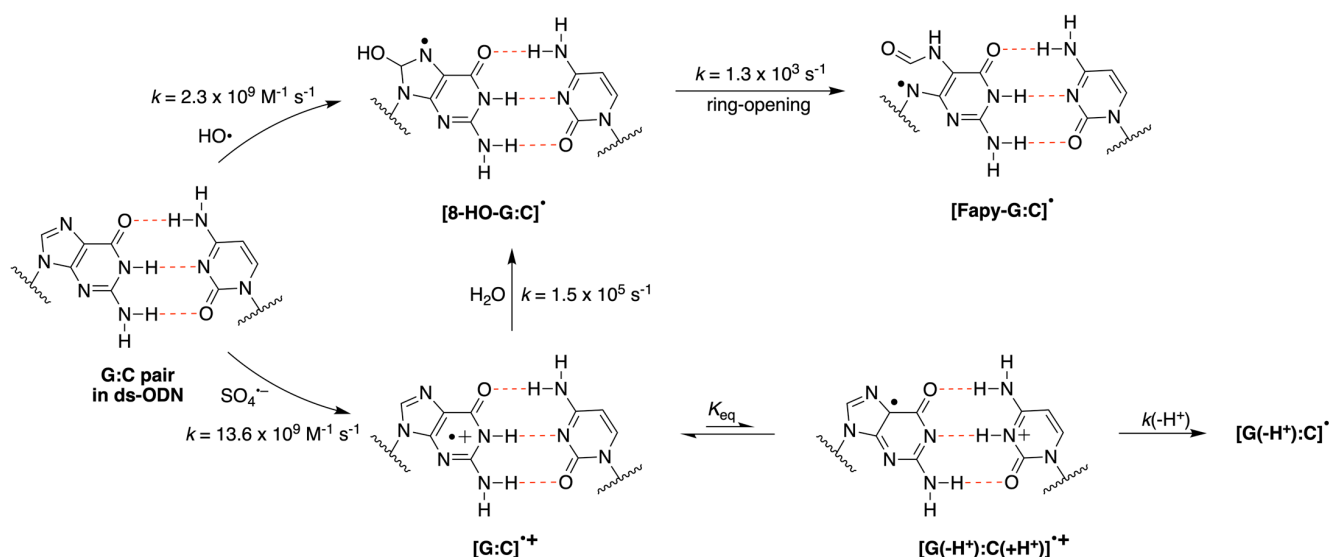


Figure 8. Proposed reaction mechanism for the reaction of HO^\bullet and $\text{SO}_4^{\bullet-}$ with the ds-ODN of the palindromic 5'-d(GCGCGC)-3' in deoxygenated aqueous solutions. The reported rate constants for the reactions of HO^\bullet and $\text{SO}_4^{\bullet-}$ are calculated for a G:C pair in alternating GC oligonucleotides.

On the other hand, the reaction of $\text{SO}_4^{\bullet-}$ with ds-ODN, reported in Figure 3, can simply be rationalized as follows: one-electron oxidation of ds-ODN followed by the hydration of $[G:C]^{\bullet+}$ to give $[8\text{-HOG:C}]^\bullet$ with a pseudo-first-order rate constant of $k(\text{H}_2\text{O}) = 1.5 \times 10^5 \text{ s}^{-1}$ (Figure 8). Indeed, Figure 4 shows that the absorption spectra of both HO^\bullet and $\text{SO}_4^{\bullet-}$ with ds-ODN (taken at 1000 μs after the pulse) are similar in

terms of features and intensity, taking into consideration the radiation chemical yields (G) of the two reactive species. Moreover, the kinetics of disappearance of both transients followed similar first-order kinetics, which we tentatively assigned to the ring opening of [8-HOG:C] \bullet with the formation of [Fapy-G:C] \bullet (Figure 8). It is worth mentioning that the reported rate constants regarding the water trapping of $G^{\bullet+}$ in ds-ODN are only estimated values [30]. The value of $k(\text{H}_2\text{O}) = 6 \times 10^4 \text{ s}^{-1}$ was calculated for the guanine radical cation in the GGG sequence via fitting using known charge transfer rates and the product yields at pH 7. The water trapping rates vary substantially, with $G^{\bullet+}$ being more reactive than $GG^{\bullet+}$ and pH-dependent. All together, our experimental values regarding water trapping fit very well with these considerations [30]. It is worth mentioning that the $G^{\bullet+}$ in the single-stranded ODN 5'-d(TCGCT) at pH 2.5, where the transient exists in the form of a radical cation, decays with a pseudo-first-order rate constant of $k(\text{H}_2\text{O}) = 3.3 \times 10^2 \text{ s}^{-1}$ [76].

The above proposal requires further consideration with respect to the spectrum shape of one-electron oxidized ds-ODN and the role of the well-known deprotonation of [G:C] $\bullet+$ in the case of the palindromic 5'-d(GCGCGC)-3'. As mentioned in the introduction, the primary damage in one-electron-oxidizing DNA is localized at Gs, which have the lowest oxidation potential. Since the earliest works in this field, it has been proposed that, in the [G:C] $\bullet+$ pair, the proton is not directly lost from $G^{\bullet+}$ to the aqueous phase but remains within the hydrogen-bonded interaction with the cytosine N3 atom [77]. ESR studies on a variety of ds-ODNs have indicated that a prototropic equilibrium [G:C] $\bullet+ \rightleftharpoons [G(-H^+):C(+H^+)]\bullet+$ should be established at ambient temperature (Figure 8) and that the proton is entirely transferred at 77 K [26]. The reaction of $\text{SO}_4^{\bullet-}$ of a variety of ds-ODNs containing G, GG, and GGG sequences has been reported in pulse radiolysis studies [42,78]. In an earlier work [78], the biphasic decay of [G:C] $\bullet+$ was attributed to the shift of a proton from the N1 in $G^{\bullet+}$ to the N3 of C, followed by the release of the proton into the solution. A few years later, the same group analyzed the optical spectra and the kinetics of eleven ds-ODNs with different sequences at 625 nm (11mer to 13mer ds-ODNs) and proposed that the monophasic decay of [G:C] $\bullet+ \rightleftharpoons [G(-H^+):C(+H^+)]\bullet+$ is associated with the release of the proton into the solution [42]. The rate constant for deprotonation was dependent on the ds-ODN sequence, varying in the range of $0.3\text{--}2 \times 10^7 \text{ s}^{-1}$, as observed by monitoring the transient at 625 nm. One of the sequences particularly relevant to the present work contains alternating GC sequences, the 11-mer 5'-d(CGCGCGCGCGC)-3' and its complementary strand, which have been associated with a faster rate constant of $2 \times 10^7 \text{ s}^{-1}$. Unfortunately, no data are shown for this ds-ODN. In our experiment (see Figure 3, red spectrum), the transient absorbance at 625 nm is close to zero, whereas we attribute the decay at 330 nm with $k = 1.5 \times 10^5 \text{ s}^{-1}$ to the hydration of [G:C] $\bullet+$. In this context, it is also worth mentioning that our theoretical results indicate the delocalization of positive charge over the central guanines on the two stacked base pairs (see Figure 6), suggesting that the K_{eq} in Figure 8 may be shifted strongly to the left since the positive charge in the palindromic 5'-d(GCGCGC)-3' sequence may be delocalized over the whole ds sequence or part (the central one) of it.

The one-electron oxidation of ds-ODN of 30-mer 5'-CGTACTCTTTGGTGG GTCGGTTCTTTCTAT-3' (G, GG, and GGG sequences) and its complementary strand by $\text{SO}_4^{\bullet-}$ was studied via laser flash photolysis by the authors of [43]. In this study, the $\text{SO}_4^{\bullet-}$ was produced via the photolysis of $\text{S}_2\text{O}_8^{2-}$ using 308 nm laser pulses, and the transient species was observed after the complete decay of $\text{SO}_4^{\bullet-}$ (5 μs), which was assigned to $G(\text{N1-H})\bullet$ and characterized by a narrow absorption band at 312 nm and two less intense bands near 390 and 510 nm [30,43]. The decay of $G(\text{N1-H})\bullet$ was biphasic, with one component decaying with a lifetime of $\sim 2.2 \text{ ms}$ and the other one with a lifetime of $\sim 0.18 \text{ s}$. The authors proposed that the equilibrium [G:C] $\bullet+ \rightleftharpoons [G(-H^+):C(+H^+)]\bullet+$ allows for the hydration and subsequent formation of 8-oxoG:C. The same ds-ODN were studied using photoionization via the direct absorption of low-energy photons, and the spectra at 5 μs are the same as above [45].

Our spectrum regarding the one-electron-oxidized palindromic 5'-d(GCGCGC)-3' sequence registered at 800 ns (Figure 3) shows a completely different shape of the G(N1-H)[•] neutral radical. Based on the described calculations, we assigned the species to [G:C]^{•+} that may be stabilized by delocalization over the whole double strand or over a part (the central one) of it. Indeed, the calculated spectral shape agree very well with the experimental one, cf. Figure 7. The fact that the absorption peak is predicted at much shorter wavelengths than the observed one (ca. 70 nm) is a well-known failure of TDDFT, irrespective of the adopted functional [46,67]. Here, the problem is further exacerbated by the large size of the system considered in computations (see Figure 6), but with sugar phosphate moieties replaced by methyl groups. Indeed, the most intense transition predicted at ca. 260 nm corresponded to the 56th excited state, and our TDDFT computations considered only 65 excited states; therefore, the computed transition energies are highly inaccurate at shorter wavelengths. Interestingly, the alternating GC sequence in duplexes has been previously studied using different techniques. The transient species generated via the direct absorption of the low-energy UV irradiation of ds-ODN palindromic 5'-GCGCGCGCGC-3' and register at 100 μs was assigned to G(N1-H)[•] [44]. This spectrum is very similar to our green spectrum in Figure 3, which we assigned to the HO[•]-adduct, i.e., [8-oxo-G:C][•].

5. Conclusions

In this work, we evaluated the reactivities of HO[•] and SO₄^{•-} with respect to the alternating GC double-stranded 5'-d(GCGCGC)-3' using time-resolved spectroscopy at a nanosecond timescale. The assignment of transient species was corroborated by a tailored computational study. A reaction with SO₄^{•-} results in the formation of the ds-ODN^{•+}, where the electron hole is delocalized over the whole or part of the alternating GC sequence. This is a new type of electron hole stabilization in CG-rich sequences of DNA. Indeed, the ODN^{•+} prefers the reaction with water ($k = 1.5 \times 10^5 \text{ s}^{-1}$) instead of the deprotonation usually observed in other studies. The neutral radical [8-oxo-G:C][•] is a common transient of both oxidizing species (Figure 8). The biological implications of the proposed double-stranded GC alternating sequences regarding hole delocalization in DNA pertain to the generation of guanine damage.

Supplementary Materials: The following supporting information can be downloaded at: <https://www.mdpi.com/article/10.3390/biom13101493/s1>, Figure S1: Analytical SAX HPLC chromatograms of purified ODNs; Figure S2: Melting curves of ds-ODN; Figure S3: Optimized geometry (PCM/B3LYP/6-311++G**) of SO₄^{•-} radical anion, including its first solvation shell; Figure S4: Isosurface contour plots of the HOMO and LUMO of [meG:C^{me}/meC:G^{me}]^{•+} in both levels of theory (B3LYP and CAM-B3LYP); Table S1: Melting points (T_m) of the ds-ODN in different buffer conditions; Table S2: Predicted energy changes (ΔE, kcal/mol) for the addition of SO₄^{•-} to the G:C pair in water; spectroscopic properties, wavelengths, and oscillator strengths of the radical adducts in water; Table S3: Comparative analysis of predicted (PCM/TD-B3LYP/TZVP) UV/vis transitions of meG^{•+} and [meG:C^{me}]^{•+}; Table S4: Comparative analysis of predicted (PCM/TD-B3LYP/TZVP) transitions of [meG:C^{me}]^{•+} and [meG:C^{me}/meC:G^{me}]^{•+}; Table S5: Predicted (PCM/TD-CAM-B3LYP/TZVP) low-energy transitions of [meG:C^{me}/meC:G^{me}]^{•+}.

Author Contributions: Conceptualization, C.C. and A.P.; methodology, C.C., K.B. and A.P.; software, A.C. and A.P.; validation, C.C., K.B. and A.P.; formal analysis, A.M. and A.C.; investigation, A.M. and A.C.; data curation, C.C. and A.P.; writing—original draft preparation, C.C., K.B. and A.P.; writing—review and editing, C.C.; supervision, C.C. and A.P. All authors have read and agreed to the published version of the manuscript.

Funding: This research article received no external funding.

Institutional Review Board Statement: Not applicable.

Informed Consent Statement: Not applicable.

Data Availability Statement: The data presented in this study are available in this article and the Supplementary Materials.

Acknowledgments: The authors acknowledge Luciano Cellai for his role in introducing some of us in the field of oligonucleotide chemical biology and for contributing to fruitful discussions. We also thank Gabriel Kciuk and Mila D'Angelantonio for providing technical assistance and contributing to discussions.

Conflicts of Interest: The authors declare no conflict of interest.

References

1. Sies, H.; Jones, D.P. Reactive oxygen species (ROS) as pleiotropic physiological signalling agents. *Nat. Rev. Mol. Cell. Biol.* **2020**, *21*, 363–383.
2. Dizdaroglu, M.; Lloyd, R.S. *DNA Damage, DNA Repair and Disease*; Royal Society of Chemistry: Croydon, UK, 2021.
3. Chatgililoglu, C.; Ferreri, C.; Krokidis, M.G.; Masi, A.; Terzidis, M.A. On the relevance of hydroxyl radical to purine DNA damage. *Free Radic. Res.* **2021**, *55*, 384–404. [[CrossRef](#)] [[PubMed](#)]
4. Halliwell, B.; Adhikary, A.; Dingfelder, M.; Dizdaroglu, M. Hydroxyl radical is a significant player in oxidative DNA damage in vivo. *Chem. Soc. Rev.* **2021**, *50*, 8355–8360. [[CrossRef](#)] [[PubMed](#)]
5. Von Sonntag, C. *Free-Radical-Induced DNA Damage and Its Repair—A Chemical Perspective*; Springer Science: Berlin/Heidelberg, Germany, 2006.
6. Bergeron, F.; Auvre, F.; Radicella, J.P.; Ravanat, J.-L. HO radicals induce an unexpected high proportion of tandem base lesions refractory to repair by DNA glycosylases. *Proc. Natl. Acad. Sci. USA* **2010**, *107*, 5528–5533. [[CrossRef](#)] [[PubMed](#)]
7. Ravanat, J.-L.; Breton, J.; Douki, T.; Gasparutto, D.; Grand, A.; Rachidi, W.; Sauvaigo, S. Radiation-mediated formation of complex damage to DNA: A chemical aspect overview. *Br. J. Radiol.* **2014**, *87*, 20130715. [[CrossRef](#)]
8. Chatgililoglu, C.; Eriksson, L.A.; Krokidis, M.G.; Masi, A.; Wang, S.-D.; Zhang, R. Oxygen dependent purine lesions in double-stranded oligodeoxynucleotides: Kinetic and computational studies highlight the mechanism for 5',8-cytopurine formation. *J. Am. Chem. Soc.* **2020**, *142*, 5825–5833. [[CrossRef](#)]
9. Douki, T.; Rivière, J.; Cadet, J. DNA tandem lesions containing 8-oxo-7,8-dihydroguanine and formamido residues arise from intramolecular addition of thymine peroxy radical to guanine. *Chem. Res. Toxicol.* **2002**, *15*, 445–454. [[CrossRef](#)]
10. Robert, G.; Wagner, J.R. Tandem lesions arising from 5-(uracilyl)methyl peroxy radical addition to guanine: Product analysis and mechanistic studies. *Chem. Res. Toxicol.* **2020**, *33*, 565–575. [[CrossRef](#)]
11. Dizdaroglu, M.; Kirkali, G.; Jaruga, P. Formamidopyrimidines in DNA: Mechanisms of formation, repair, and biological effects. *Free Radic. Biol. Med.* **2008**, *45*, 1610–1621.
12. Greenberg, M.M. The formamidopyrimidines: Purine lesions formed in competition with 8-oxopurines from oxidative stress. *Acc. Chem. Res.* **2012**, *45*, 588–597. [[CrossRef](#)]
13. Ryan, B.J.; Yang, H.; Bacurio, J.H.T.; Smith, M.R.; Basu, A.K.; Marc, M.; Greenberg, M.M.; Freudenthal, B.D. Structural Dynamics of a Common Mutagenic Oxidative DNA Lesion in Duplex DNA and during DNA Replication. *J. Am. Chem. Soc.* **2022**, *144*, 8054–8065. [[CrossRef](#)] [[PubMed](#)]
14. Oliveira-Brett, A.M.; Piedade, J.A.P.; Silva, L.A.; Diclescu, V.C. Voltammetric Determination of All DNA Nucleotides. *Anal. Biochem.* **2004**, *332*, 321–329. [[CrossRef](#)]
15. Brotons, A.; Mas, L.A.; Metters, J.P.; Banks, C.E.; Iniesta, J. Voltammetric Behaviour of Free DNA Bases, Methylcytosine and Oligonucleotides at Disposable Screen Printed Graphite Electrode Platforms. *Analyst* **2013**, *138*, 5239–5249. [[CrossRef](#)]
16. Pluharová, E.; Slavíček, P.; Jungwirth, P. Modeling Photoionization of Aqueous DNA and Its Components. *Acc. Chem. Res.* **2015**, *48*, 1209–1217. [[CrossRef](#)] [[PubMed](#)]
17. Peluso, A.; Caruso, T.; Landi, A.; Capobianco, A. The Dynamics of Hole Transfer in DNA. *Molecules* **2019**, *24*, 4044. [[CrossRef](#)] [[PubMed](#)]
18. Genereux, J.C.; Barton, J.K. Mechanisms for DNA Charge Transport. *Chem. Rev.* **2010**, *110*, 1642–1662.
19. Kawai, K.; Majima, T. Hole Transfer Kinetics of DNA. *Acc. Chem. Res.* **2013**, *46*, 2616–2625. [[CrossRef](#)]
20. Zwang, T.J.; Tse, E.C.M.; Barton, J.K. Sensing DNA through DNA Charge Transport. *ACS Chem. Biol.* **2018**, *13*, 1799–1809. [[CrossRef](#)]
21. Lewis, F.D.; Young, R.M.; Wasielewski, M.R. Tracking Photoinduced Charge Separation in DNA: From Start to Finish. *Acc. Chem. Res.* **2018**, *51*, 1746–1754. [[CrossRef](#)]
22. Caruso, T.; Carotenuto, M.; Vasca, E.; Peluso, A. Direct Experimental Observation of the Effect of the Base Pairing on the Oxidation Potential of Guanine. *J. Am. Chem. Soc.* **2005**, *127*, 15040–15041. [[CrossRef](#)]
23. Caruso, T.; Capobianco, A.; Peluso, A. The Oxidation Potential of Adenosine and Adenosine-Thymidine Base-Pair in Chloroform Solution. *J. Am. Chem. Soc.* **2007**, *129*, 15347–15353. [[CrossRef](#)] [[PubMed](#)]
24. Capobianco, A.; Caruso, T.; Peluso, A. Hole Delocalization over Adenine Tracts in Single Stranded DNA Oligonucleotides. *Phys. Chem. Chem. Phys.* **2015**, *17*, 4750–4756. [[CrossRef](#)] [[PubMed](#)]
25. Capobianco, A.; Caruso, T.; D'Ursi, A.M.; Fusco, S.; Masi, A.; Scrima, M.; Chatgililoglu, C.; Peluso, A. Delocalized Hole Domains in Guanine-Rich DNA Oligonucleotides. *J. Phys. Chem. B* **2015**, *119*, 5462–5466. [[CrossRef](#)] [[PubMed](#)]
26. Adhikary, A.; Khanduri, D.; Sevilla, M.D. Direct observation of the hole protonation state and hole localization site in DNA-oligomers. *J. Am. Chem. Soc.* **2009**, *131*, 8614–8619. [[CrossRef](#)]

27. Shukla, L.I.; Adhikary, A.; Pazdro, R.; Becker, D.; Sevilla, M.D. Formation of 8-oxo-7,8-dihydroguanine-radicals in γ -irradiated DNA by multiple one-electron oxidations. *Nucl. Acids Res.* **2004**, *32*, 6565–6574. [[CrossRef](#)]
28. Becker, D.; Kumar, A.; Adhikary, A.; Sevilla, M.D. Gamma-and Ion-beam DNA Radiation Damage: Theory and Experiments. In *DNA Damage, DNA Repair and Disease*; Royal Society of Chemistry: Croydon, UK, 2021; Chapter 31; pp. 426–457.
29. Barnett, R.N.; Bongiorno, A.; Cleveland, C.L.; Joy, A.; Landman, U.; Schuster, G.B. Oxidative Damage to DNA: Counterion-Assisted Addition of Water to ionized DNA. *J. Am. Chem. Soc.* **2006**, *128*, 10795–10800. [[CrossRef](#)]
30. Giese, B.; Spichty, M. Long Distance Charge Transport through DNA: Quantification and Extension of the Hopping Model. *ChemPhysChem* **2000**, *1*, 195–198. [[CrossRef](#)]
31. Chatgililoglu, C. The Two Faces of the Guanyl Radical: Molecular Context and Behavior. *Molecules* **2021**, *26*, 3511. [[CrossRef](#)]
32. Cadet, J.; Wagner, J.R. Oxidatively generated base damage to cellular DNA by hydroxyl radical and one-electron oxidants: Similarities and differences. *Arch. Biochem. Biophys.* **2014**, *557*, 47–54.
33. Chatgililoglu, C.; D'Angelantonio, M.; Guerra, M.; Kaloudis, P.; Mulazzani, Q.G. A reevaluation of the ambident reactivity of guanine moiety towards hydroxyl radicals. *Angew. Chem. Int. Ed.* **2009**, *48*, 2214–2217. [[CrossRef](#)]
34. Chatgililoglu, C.; D'Angelantonio, M.; Kciuk, G.; Bobrowski, K. New insights into the reaction paths of hydroxyl radicals with 2'-deoxyguanosine. *Chem. Res. Toxicol.* **2011**, *24*, 2200–2206. [[CrossRef](#)] [[PubMed](#)]
35. Chatgililoglu, C.; Caminal, C.; Altieri, A.; Vougioukalakis, G.C.; Mulazzani, Q.G.; Gimisis, T.; Guerra, M. Tautomerism in the guanyl radicals. *J. Am. Chem. Soc.* **2006**, *128*, 13796–13805. [[CrossRef](#)]
36. Chatgililoglu, C.; Bazzanini, R.; Jimenez, L.B.; Miranda, M.A. (5'S)- and (5'R)-5',8-cyclo-2'-deoxyguanosine: Mechanistic insights on the 2'-deoxyguanosin-5'-yl radical cyclization. *Chem. Res. Toxicol.* **2007**, *20*, 1820–1824. [[CrossRef](#)] [[PubMed](#)]
37. Aravindakumar, C.T.; Schuchmann, M.N.; Rao, B.S.M.; von Sonntag, J.; von Sonntag, C. The Reactions of Cytidine and 2'-Deoxycytidine with $\text{SO}_4^{\bullet-}$ Revisited. Pulse Radiolysis and Product Studies. *Org. Biomol. Chem.* **2003**, *1*, 401–408. [[CrossRef](#)] [[PubMed](#)]
38. Wang, Y.; Zhao, H.; Yang, C.; Jie, J.; Dai, X.; Zhou, Q.; Liu, K.; Song, D.; Su, H. Degradation of Cytosine Radical Cations in 2'-Deoxycytidine and in i-Motif DNA: Hydrogen-Bonding Guided Pathways. *J. Am. Chem. Soc.* **2019**, *141*, 1970–1979. [[CrossRef](#)]
39. Peng, H.; Jie, J.; Mortimer, I.P.; Ma, Z.; Su, H.; Greenberg, M.M. Reactivity and DNA Damage by Independently Generated 2'-Deoxycytidin-N4-yl Radical. *J. Am. Chem. Soc.* **2021**, *143*, 14738–14747. [[CrossRef](#)] [[PubMed](#)]
40. Arhondakis, S.; Auletta, F.; Torelli, G.; D'Onofrio, G. Base composition and expression level of human genes. *Gene* **2004**, *325*, 165–169. [[CrossRef](#)]
41. Bernaola-Galván, P.; Carpena, P.; Gómez-Martín, C.; Oliver, J.L. Compositional Structure of the Genome: A Review. *Biology* **2023**, *12*, 849.
42. Kobayashi, K.; Yamagami, R.; Tagawa, S. Effect of base sequence and deprotonation of guanine cation radical in DNA. *J. Phys. Chem. B* **2008**, *112*, 10752–10757. [[CrossRef](#)]
43. Rokhlenko, Y.; Cadet, J.; Geacintov, N.E.; Shafirovich, V. Mechanistic aspects of hydration of guanine radical cations in DNA. *J. Am. Chem. Soc.* **2014**, *136*, 5956–5962.
44. Banyasz, A.; Martínez-Fernández, L.; Improta, R.; Ketola, T.-M.; Balty, C.; Markovitsi, D. Radicals generated in alternating guanine cytosine duplexes by direct absorption of low-energy UV radiation. *Phys. Chem. Chem. Phys.* **2018**, *20*, 21381–21389. [[CrossRef](#)] [[PubMed](#)]
45. Balanikas, E.; Banyasz, A.; Baldacchino, G.; Markovitsi, D. Populations and Dynamics of Guanine Radicals in DNA strands—Direct versus Indirect Generation. *Molecules* **2019**, *24*, 2347. [[CrossRef](#)] [[PubMed](#)]
46. Banyasz, A.; Martínez-Fernández, L.; Balty, C.; Perron, M.; Douki, T.; Improta, R.; Markovitsi, D. Absorption of Low-Energy UV Radiation by Human Telomere G-Quadruplexes Generates Long-Lived Guanine Radical Cations. *J. Am. Chem. Soc.* **2017**, *139*, 10561–10568. [[CrossRef](#)]
47. Masi, A.; Sabbia, A.; Ferreri, C.; Manoli, F.; Lai, Y.; Laverde, E.; Liu, Y.; Krokidis, M.G.; Chatgililoglu, C.; Faraone Mennella, M.R. Diastereomeric Recognition of 5',8-cyclo-2'-Deoxyadenosine Lesions by Human Poly(ADP-ribose) Polymerase 1 in a Biomimetic Model. *Cells* **2019**, *8*, 116. [[CrossRef](#)] [[PubMed](#)]
48. Bobrowski, K. Free radicals in chemistry, biology and medicine: Contribution of radiation chemistry. *Nukleonika* **2005**, *50* (Suppl. S3), S67–S76.
49. Janata, E.; Schuler, R.H. Rate constant for scavenging e_{aq}^- in N_2O -saturated solutions. *J. Phys. Chem.* **1982**, *86*, 2078–2084. [[CrossRef](#)]
50. Stephens, P.J.; Devlin, F.J.; Chabalowski, C.F.; Frisch, M.J. Ab Initio Calculation of Vibrational Absorption and Circular Dichroism Spectra Using Density Functional Force Fields. *J. Phys. Chem.* **1994**, *98*, 11623–11627. [[CrossRef](#)]
51. Tomasi, J.; Mennucci, B.; Cammi, R. Quantum mechanical continuum solvation models. *Chem. Rev.* **2005**, *105*, 2999–3094.
52. Lu, X.J.; Olson, W.K. 3DNA: A Versatile, Integrated Software System for the Analysis, Rebuilding and Visualization of Three-dimensional Nucleic-Acid Structures. *Nat. Protoc.* **2008**, *3*, 1213–1227.
53. Grimme, S.; Ehrlich, S.; Goerigk, L. Effect of the Damping Function in Dispersion Corrected Density Functional Theory. *J. Comput. Chem.* **2011**, *32*, 1456–1465.
54. Capobianco, A.; Velardo, A.; Peluso, A. Single-Stranded DNA Oligonucleotides Retain Rise Coordinates Characteristic of Double Helices. *J. Phys. Chem. B* **2018**, *122*, 7978–7989. [[CrossRef](#)]

55. Yanai, T.; Tew, D.P.; Handy, N.C. A New Hybrid Exchange-Correlation Functional Using the Coulomb-Attenuating Method (CAM-B3LYP). *Chem. Phys. Lett.* **2004**, *393*, 51–57. [[CrossRef](#)]
56. Frisch, M.J.; Trucks, G.W.; Schlegel, H.B.; Scuseria, G.E.; Robb, M.A.; Cheeseman, J.R.; Scalmani, G.; Barone, V.; Mennucci, B.; Petersson, G.A.; et al. *Gaussian 09*; Revision B.01; Gaussian Inc.: Wallingford, CT, USA, 2009.
57. Buxton, G.V.; Greenstock, C.L.; Helman, W.P.; Ross, A.B. Critical review of rate constants for hydrated electrons, hydrogen atoms and hydroxyl radicals (OH/O⁻) in aqueous solution. *J. Phys. Chem. Ref. Data* **1988**, *17*, 513–886. [[CrossRef](#)]
58. Buxton, G.V. An overview of the radiation chemistry of liquids. In *Radiation Chemistry: From Basics to Applications in Material and Life Sciences*; Spothem Maurizot, M., Mostafavi, M., Douki, T., Belloni, J., Eds.; EDP Sciences: Paris, France, 2008; pp. 3–16.
59. Zhang, R.; Eriksson, L.A. Effects of OH Radical Addition on Proton Transfer in the Guanine-Cytosine Base Pair. *J. Phys. Chem. B* **2007**, *111*, 6571–6576. [[CrossRef](#)] [[PubMed](#)]
60. Cerón-Carrasco, J.P.; Jacquemin, D. Interplay between hydroxyl radical attack and H-bond stability in guanine–cytosine. *RCS Adv.* **2012**, *2*, 11867–11875. [[CrossRef](#)]
61. Li, M.; Diao, L.; Liao, X.; Kou, L.; Lu, W. DFT study on addition reaction mechanism of guanine-cytosine base pair with OH radical. *J. Phys. Org. Chem.* **2015**, *28*, 437–444.
62. Ambrosio, F.; Miceli, G.; Pasquarello, A. Redox levels in aqueous solution: Effect of van der Waals interactions and hybrid functionals. *Chem. Phys.* **2015**, *143*, 244508. [[CrossRef](#)]
63. Adriaanse, C.; Cheng, J.; Chau, V.; Sulpizi, M.; VandeVondele, J.; Sprik, M. Aqueous Redox Chemistry and the Electronic Band Structure of Liquid Water. *J. Phys. Chem. Lett.* **2012**, *3*, 3411–3415. [[CrossRef](#)]
64. Capobianco, A.; Russo, A.; Lattanzi, A.; Peluso, A. On the Mechanism of Asymmetric Epoxidation of Enones Catalyzed by α,α -L-Diarylprolinols: A Theoretical Insight. *Adv. Synth. Catal.* **2012**, *354*, 2789–2796. [[CrossRef](#)]
65. Zhang, P.; Wang, Q.; Fang, Y.; Chen, W.; Kirchon, A.A.; Baci, M.; Feng, M.; Sharma, V.K.; Zhou, H.-C. 7—Metal-organic frameworks for capture and degradation of organic pollutants. In *Metal-Organic Frameworks (MOFs) for Environmental Applications*; Ghosh, S.K., Ed.; Elsevier: Amsterdam, The Netherlands, 2019; pp. 203–229.
66. Fukuzumi, S.; Miyao, H.; Ohkubo, K.; Suenobu, T. Electron-Transfer Oxidation Properties of DNA Bases and DNA Oligomers. *J. Phys. Chem. A* **2005**, *109*, 3285–3294.
67. Capobianco, A.; Carotenuto, M.; Caruso, T.; Peluso, A. The Charge-Transfer Band of an Oxidized Watson-Crick Guanosine-Cytidine Complex. *Angew. Chem. Int. Ed.* **2009**, *48*, 9526–9528. [[CrossRef](#)] [[PubMed](#)]
68. Kumar, A.; Sevilla, M.D. Excited States of One-Electron Oxidized Guanine-Cytosine Base Pair Radicals: A Time Dependent Density Functional Theory Study. *J. Phys. Chem. A* **2019**, *123*, 3098–3108. [[CrossRef](#)] [[PubMed](#)]
69. Harris, M.A.; Mishra, A.K.; Young, R.M.; Brown, K.E.; Wasielewski, M.R.; Lewis, F.D. Direct Observation of the Hole Carriers in DNA Photoinduced Charge Transport. *J. Am. Chem. Soc.* **2016**, *138*, 5491–5494. [[CrossRef](#)]
70. Capobianco, A.; Caruso, T.; Celentano, M.; La Rocca, M.V.; Peluso, A. Proton Transfer in Oxidized Adenosine Self-Aggregates. *J. Chem. Phys.* **2013**, *139*, 145101. [[CrossRef](#)] [[PubMed](#)]
71. Sugiyama, H.; Saito, I. Theoretical Studies of GG-Specific Photocleavage of DNA via Electron Transfer: Significant Lowering of Ionization Potential and 5'-Localization of HOMO of Stacked GG Bases in B-Form DNA. *J. Am. Chem. Soc.* **1996**, *118*, 7063–7068. [[CrossRef](#)]
72. Capobianco, A.; Landi, A.; Peluso, A. Modeling DNA Oxidation in Water. *Phys. Chem. Chem. Phys.* **2017**, *19*, 13571–13578. [[CrossRef](#)]
73. Conwell, E.M.; Bloch, S.M.; McLaughlin, P.M.; Basko, D.M. Duplex Polarons in DNA. *J. Am. Chem. Soc.* **2007**, *129*, 9175–9181. [[CrossRef](#)]
74. Schüssler, H.; Navaratnam, S.; Distel, L. Rate constants for the reactions of DNA with hydrated electrons and with OH-radicals. *Radiat. Phys. Chem.* **2005**, *73*, 163–168. [[CrossRef](#)]
75. Chatgililoglu, C.; Krokidis, M.G.; Masi, A.; Barata-Vallejo, S.; Ferreri, C.; Terzidis, M.A.; Szreder, T.; Bobrowski, K. New insights into the reaction paths of hydroxyl radicals with purine moieties in DNA and double-stranded oligonucleotides. *Molecules* **2019**, *24*, 3860. [[CrossRef](#)]
76. Rokhlenko, Y.; Geacintov, N.E.; Shafirovich, V. Lifetimes and reaction pathways of guanine radical cations and neutral guanine radicals in an oligonucleotide in aqueous solutions. *J. Am. Chem. Soc.* **2012**, *134*, 4955–4962. [[CrossRef](#)]
77. Steenken, S. Purine bases, nucleosides, and nucleotides: Aqueous solution redox chemistry and transformation reactions of their radical cations and e⁻ and OH adducts. *Chem. Rev.* **1989**, *89*, 503–520. [[CrossRef](#)]
78. Kobayashi, K.; Tagawa, S. Direct Observation of Guanine Radical Cation Deprotonation in Duplex DNA Using Pulse Radiolysis. *J. Am. Chem. Soc.* **2003**, *125*, 10213–10218. [[CrossRef](#)] [[PubMed](#)]

Disclaimer/Publisher's Note: The statements, opinions and data contained in all publications are solely those of the individual author(s) and contributor(s) and not of MDPI and/or the editor(s). MDPI and/or the editor(s) disclaim responsibility for any injury to people or property resulting from any ideas, methods, instructions or products referred to in the content.